Sintered porous hydroxyapatites with intrinsic osteoinductive activity: geometric induction of bone formation

U. Ripamonti[a*], J. Crooks[a] and A.N. Kirkbride[b]

Sintered hydroxyapatites induce bone formation in adult baboons *via* intrinsic osteoinductivity regulated by the geometry of the substratum. Bone is thereby formed without exogenous bone morphogenetic proteins (BMPs), well-characterized inducers of bone formation. Monolithic discs of sintered hydroxyapatite, fabricated with concavities of 800 and 1600 μm diameter on both planar surfaces, were implanted in the rectus abdominis of the baboon (*Papio ursinus*). Histology on days 30 and 90 revealed *de novo* generation of bone exclusively within the concavities of the substratum. Porous hydroxyapatites were subsequently fabricated by impregnating polyurethane foams with slurry preparations of powdered hydroxyapatite, so that porous spaces formed by the coalescence of repetitive sequences of concavities. Artefacts were sintered in rod and disc configurations for implantation in heterotopic intramuscular sites and orthotopic calvarial sites, respectively. In four specimens, bone had formed in concavities of the substratum 30 days after implantation in the rectus abdominis. On day 90, bone morphogenesis with associated marrow had occurred in 33 specimens (41 %). Calvarial specimens showed substantial bone formation, culminating in complete penetration of bone within the porous spaces. On day 30, the immunolocalization of BMP family members (BMP-3 and OP-1/BMP-7) in cellular material at the hydroxyapatite interface suggests that the sintered ceramic may act as a solid-state matrix for adsorption of endogenously produced BMPs. These experiments demonstrate intrinsic osteoinductivity by monolythic and porous sintered hydroxyapatites implanted in heterotopic sites of adult primates, and that the geometry of the substratum profoundly regulates the expression of the osteogenic phenotype. The incorporation of specific biological activities into biomaterials achieved by manipulating the geometry of the substratum, defined as geometric induction of bone formation, will help engineer morphometric responses for therapeutic osteogenesis in clinical contexts.

Tissue engineering of bone requires three key components: a soluble osteoinductive signal, a suitable insoluble substratum that delivers the signal and acts as a scaffold for new bone to form, and responding host cells capable of differentiation into bone cells.[1-3] The signals responsible for osteoinduction are the bone morphogenetic proteins (BMP-2 to BMP-14) and osteogenic proteins 1 and 2 (OP-1 and OP-2, also known as BMP-7 and BMP-8), that regulate cartilage and bone differentiation *in vivo*.[3-7] A striking function of BMPs/OPs is their capacity to induce *de novo* bone differentiation when implanted in heterotopic (extraskeletal) sites of animals.[3-7] From a therapeutic perspective, a carrier substratum is required for local delivery of recombinant human (h)BMPs/OPs to evoke a desired osteogenic response, since it is the composite of a biomaterial carrier together with hBMPs/OPs that triggers the bone-induction cascade.[1,3,5,7] Thus, a critical issue in tissue engineering and morphogenesis of bone is the development of osteoinductive biomaterials capable of optimizing hBMPs/OPs delivery and biological activity.

It is important to differentiate an osteoinductive biomaterial from an osteoconductive one. The former bears osteogenic activity *per se*.[2] Its discriminatory action is osteogenesis. An osteoconductive biomaterial, on the other hand, is not inherently osteoinductive. Its function lies in its capacity to guide and direct the growth of bone at its interfaces and to achieve osteointegration after implantation in orthotopic (intraskeletal) sites.[8,9] The test for osteoinductivity is the histological evidence of bone formation in heterotopic sites in animals. While the preparation of composites of osteoconductive biomaterials and hBMPs/OPs will result in the formulation of osteoinductive biomaterials, an exciting novel concept in tissue engineering is the generation of bone by the implantation of biomaterials that can induce desired and specific responses from the host tissues without the addition of exogenously applied hBMPs/OPs.

We have previously reported the remarkable morphogenesis of bone in a specific configuration of a porous hydroxyapatite in the absence of exogenously applied BMPs/OPs when implanted in heterotopic sites of the adult baboon (*Papio ursinus*).[10-13] These studies suggested that the porous hydroxyapatite acts as a solid substratum for adsorption, storage and controlled release of endogenously produced BMPs/OPs, which locally initiate bone formation.[10-13] This apparently unique endogenously-regulated mechanism(s) to initiate bone induction in primates has been exploited to test the effect of pore size and geometry of the hydroxyapatite substratum on bone morphogenesis.[14] It is noteworthy that in these experiments in heterotopic sites of the baboon, bone was only found in porous hydroxyapatite in block configuration.[10-14] By contrast, bone did not grow in identical porous hydroxyapatite in granular form.[14] This emphasizes the importance of the geometry of the substratum as reported in earlier experiments on rodents, that showed bone did not differentiate when granular hydroxyapatite was used, even if pretreated with BMPs/OPs.[15]

The biological principles derived from these experiments in heterotopic sites of the baboon led to the hypothesis that bone may initiate in concavities rather than on convexities of the hydroxyapatite substratum. To test this hypothesis, sintered hydroxyapatite artefacts were prepared with defined concavities, incorporated either on the surface of solid blocks or assembled into porous blocks and implanted in adult baboons. Spontaneous initiation of bone formation proved to be regulated by the geometry of the concavities. This supports a novel concept in tissue engineering of bone, that is, substrata with *osteoinductive geometric configurations*, because bone morphogenesis and the generation of marrow depended on the geometry of the hydroxyapatite.

[a]Bone Research Unit, Medical Research Council/University of the Witwatersrand Medical School, 7 York Road, Parktown, Johannesburg, 2193 South Africa.
E-mail: 177ripa@chiron.wits.ac.za

[b]Division of Materials Science and Technology, CSIR, P.O. Box 395, Pretoria, 0001 South Africa.

*Author for correspondence.

Materials and methods

Preparation and sintering of hydroxyapatites

To determine the critical role of substratum geometry in bone differentiation, slurry preparations of Tribo-Corr 65–90 μm hydroxyapatite powder (Tribo Corr, South Africa) were sintered to form solid monolithic hydroxyapatite discs (20 mm in diameter, 4 mm in thickness) with a series of concavities prepared on their planar surfaces. On one surface, concavities were 1600 μm in diameter and 800 μm deep, whereas on the opposite surface, concavities were 800 and 400 μm in diameter and depth, respectively. Twenty concavities were prepared on each surface of the disc. Sintered porous hydroxyapatites were made by a sponge impregnation method.[16] Commercially available polyurethane foams, with continuous and interconnecting pores, were cut into rods 7 mm in diameter and 20 mm in length, and into discs 24 mm in diameter and 4 mm thick. Slurry preparations were made using five starting powders of hydroxyapatite: Plasma Biotal No. 3 and P120 (Plasma Biotal, England), GR 500 P (Cam Implants, The Netherlands), Plasmatex A6020 (Plasma Technik, Switzerland), and Tribo-Corr 65–90 μm. Slurries were prepared by mixing the 5 hydroxyapatite grades (70 g) with absolute ethanol (50 g), emphos PS-21A as deflocculant (1 g), and a binder/plasticizer mix (36 g) for 12 hours. The binder was made by mixing with continuous gentle agitation polyethylene glycol No. 6000 (90 g), polyvinyl butyryl (150 g), absolute ethanol (240 g) and trichloroethylene (600 g) for 24 hours to ensure complete dissolution. The slurries were aged for a further 24 hours for optimum dispersion. The prepared foam specimens were soaked in the deflocculated slurry and repeatedly compressed and expanded to ensure complete coverage of all pore walls. Excess slurry was removed by squeezing, and the coated and saturated foam was dried in air at room temperature. Artefacts were formed by heating the impregnated foams in stages to ensure the complete burning-off of all organic material and finally sintering the ceramic in a Super Kanthal furnace. Artefacts in the form of discs for implantation in baboon calvaria were 25 mm in diameter and 4 mm thick. Before insertion in the baboon, the hydroxyapatites were sterilized in an autoclave at 115 °C for 20 minutes. Chemical and physical characteristics of the starting powders of hydroxyapatite and of the final sintered artefacts were determined by X-ray diffraction (XRD) and scanning electron microscopy (SEM).

Primate models of tissue morphogenesis

Sixteen clinically healthy adult Chacma baboons *(Papio ursinus)*, with a mean weight of 25.7 ± 2.3 kg and with normal haematological and biochemical profiles, were selected from the primate colony of the University of the Witwatersrand. Selection, housing conditions and diets were as described previously.[11,17] Research protocols were approved by the Animal Ethics Screening Committee of the university. The heterotopic and orthotopic models of tissue morphogenesis by osteoinductive and osteoconductive biomaterials in the adult baboon have been described in detail.[17–22] A total of 40 monolithic hydroxyapatite discs, 20 mm in diameter and 4 mm thick, and 104 porous sintered hydroxyapatite rods, 20 mm in height and 7 mm in diameter, were implanted bilaterally in intramuscular pouches created in the rectus abdominis, 6–12 implants per animal. Four baboons were also used for the orthotopic study, to be evaluated only on day 90 after hydroxyapatite implantation. On each side of the calvaria, two full-thickness defects, 25 mm in diameter, each separated by 2.5–3.0 cm of intervening calvarial bone, were prepared with a craniotome.[18–22] In each animal, the four defects were implanted with two sintered discs prepared from Plasma Biotal No. 3 and two sintered discs prepared from Tribo Corr 65–90 μm hydroxyapatite powders as starting material, and which were selected after histological evaluation of porous sintered hydroxyapatites harvested from intramuscular sites of two baboons.

Tissue processing, histology and histomorphometry

Anaesthetized experimental animals were killed with an intravenous overdose of pentobarbitone, 6 animals on day 30 and 10 animals on day 90. Implants from the rectus abdominis were fixed in 10 % neutral buffered formaldehyde, decalcified in a formic-hydrochloric acid mixture, and double-embedded in celloidin and paraffin wax.[11–14] Serial sections, 5 μm thick, were cut in a plane perpendicular to the long axis of the hydroxyapatite rods.[10–14] Bilateral carotid perfusion and harvest of orthotopic specimens with surrounding calvaria were as described previously.[18–22] Specimen blocks were cut along the sagittal one third of the implanted discs, further fixed in 10 % neutral buffered formaldehyde, and processed as described above. Serial sections, 5 μm thick, were mounted after recording the position of the anterior and posterior interfaces of the defects with their corresponding calvarial margins. Goldner's trichrome-stained sections were examined with a Provis AX70 research microscope (Olympus Optical) equipped with a calibrated Zeiss Integration Platte II with 100 lattice points for determination, with the point counting technique,[23] of bone, fibrovascular tissue and hydroxyapatite substratum volumes. Calvarial sections were analysed at ×40, superimposing the Zeiss graticule over five sources[24] selected for histomorphometry and defined as follows: two anterior and posterior interfacial regions, two anterior and posterior internal regions and a central region. This technique allows the histomorphometric evaluation of the distribution of bone deposition across the hydroxyapatite substrata.[18,19] Each source represented a field of 7.84 mm^2.[18–22] Sections generated from the heterotopic specimens were evaluated by superimposing the Zeiss graticule over the centre of the specimen, and a single and central field of 7.84 mm^2 was analysed for each section.[11–14] Morphometry was performed on two sections per heterotopic implant, representing two levels approximately 800 μm from each other, and on two sections per orthotopic implant, representing two parasagittal levels, approximately 2 mm apart[18,19]

Immunolocalization of BMP family members

Additional sections prepared from specimens containing monolithic discs of hydroxyapatite harvested from the rectus abdominis on day 30 were cut at 5 μm, mounted on incubated silanized slides, and used for immunohistochemical staining of BMP-2, -3, -4 and OP-1 (BMP-7) using the avidin biotin immunoperoxidase technique.[25] Polyclonal anti BMP-2 antibodies (lot BUNY88), raised against *E. coli*-expressed hBMP-2, were provided by Creative BioMolecules (Hopkinton, Massachusetts) and used at a concentration of 1:200. Polyclonal anti BMP-3 and anti BMP-4 antibodies (donated by N.S. Cunningham and A.H. Reddi, Johns Hopkins University) were raised against amino acid sequences of tryptic peptides of BMP-3/osteogenin (15 amino acids from the first processed cysteine in the amino-terminal region),[26] and hBMP-4, expressed and purified as described,[27] and used at a concentration of 1:300 and 1:200, respectively. Monoclonal anti OP-1 antibodies (lot IB12, Creative BioMolecules) were prepared as described,[28] and used at a concentration of 1:80. Developing cartilage and bone served as positive control for BMP-2 and -4 antibodies, while developing

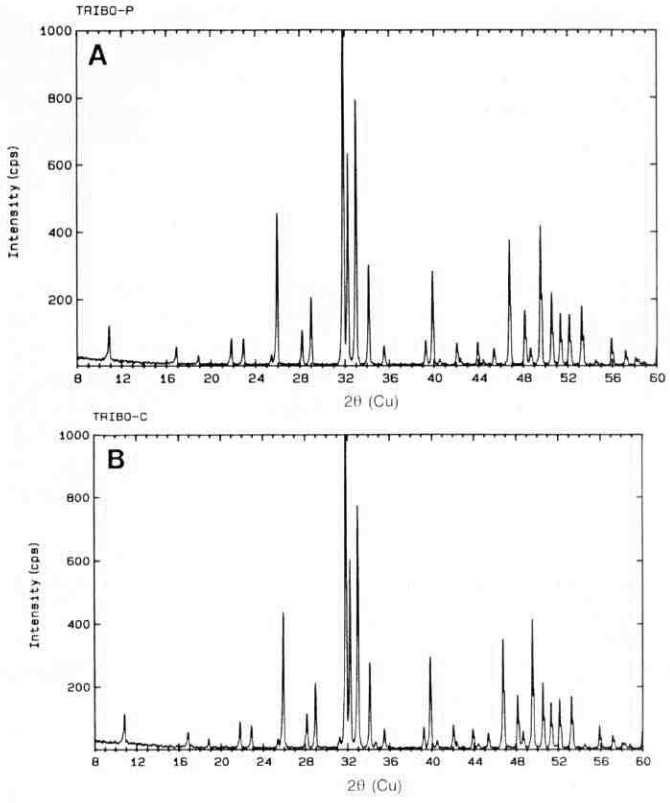

Fig. 1. X-ray diffractograms of Tribo-Corr hydroxyapatite powder (**A**) and of an experimental porous ceramic artefact (**B**) after sintering and fabrication using the foam impregnation method.

mouse lung tissue and embryonic murine kidneys served as positive control tissues for BMP-3 and OP-1 antibodies, respectively.[29,30] Antibodies were used in conjunction with anti-rabbit secondary antibody ABC kits (Vector Labs, Burlingame, California). Sections were counterstained with haematoxylin. Negative controls were provided by substituting the primary antibody with bovine serum albumin or with secondary antibody alone.

Statistical analysis

Data were analysed with the Statistical Analysis System.[31] An *F*-test was performed using the general linear models procedure for an analysis of variance with multiple interactions. Comparison of mean values was obtained using Scheffe's multiple-comparison procedure on the dependent variables included in the analysis. The critical level of statistical significance was $P < 0.05$.

Results

Chemical and physical characteristics

X-ray diffraction analysis of all precursor powder materials revealed that the hydroxyapatites were highly crystalline. Representative X-ray diffractograms of Tribo-Corr powder and of a sintered artefact are shown in Fig. 1A and Fig. 1B, respectively. SEM images of hydroxyapatite precursor powder and of a porous sintered artefact are shown in Fig. 2.

Surface geometry regulates bone differentiation in heterotopic sites

To determine intrinsic osteoinductivity imparted by surface geometry, monolithic discs of sintered hydroxyapatite, fabricated with concavities of 800 and 1600 μm diameter on both outer surfaces, were implanted in the rectus abdominis of the baboon. Histological analysis on days 30 and 90 revealed that bone formed exclusively within the concavities of the substratum (Figs 3, 4). Immunohistochemistry on paraffin-embedded sections of monolithic discs of hydroxyapatite harvested on day 30 showed localization of OP-1 (BMP-7) in newly generated collagenic fibres and cellular material emanating from the concavities of the substratum (Fig. 5B, D). BMP-3 formed adjacent to the hydroxyapatite interface (Fig. 5F). BMP-2 and -4, while immunolocalized in control tissue of developing cartilage and bone, was not detected in experimental material (not shown).

Because the start of bone formation is regulated by surface macro-geometry, porous artefacts were prepared by sintering hydroxyapatite such that spaces formed by the coalescence of concavities (Fig. 2B). On days 30 and 90 after implantation, muscular and connective tissues were firmly attached to the rods of sintered hydroxyapatite without macroscopic evidence of fibrous encapsulation. In three Plasma Biotal and one Tribo-Corr specimens, bone had formed within the concavities and in direct apposition to the hydroxyapatite substratum as early as 30 days after implantation (Fig. 6A). There was penetration of cells from adjacent large porous spaces and deposition of extracellular matrix within micro-channels and micro-lacunae of the substratum. The newly formed bone appeared to bond directly with the hydroxyapatite, anchoring into its microporosity and lacunae (Fig. 6A).

By day 90, bone morphogenesis had occurred in 33 specimens (41 %). Although the amount of bone varied considerably, its formation was extensive in four Tribo-Corr, three Plasma Biotal No. 3, five Plasma Biotal P120, two Plasmatex and five GR 500 specimens (Figs 6, 7). Bone was consistently found in concavities

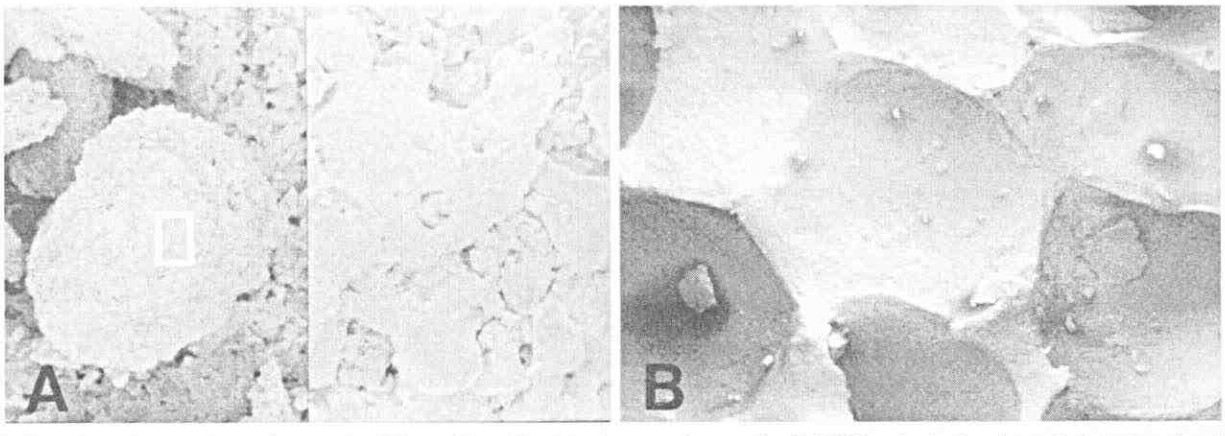

Fig. 2. **A**: Scanning electron photomicrograph of Plasma Biotal No. 3 hydroxyapatite powder; **B**: SEM analysis of a sintered artefact made of Plasma Biotal powder shows the alveolar-like pattern of the hydroxyapatite substratum and the resulting porous spaces formed by sequences of concavities with defined radii of curvature, and diameters ranging from 400–1600 µm.

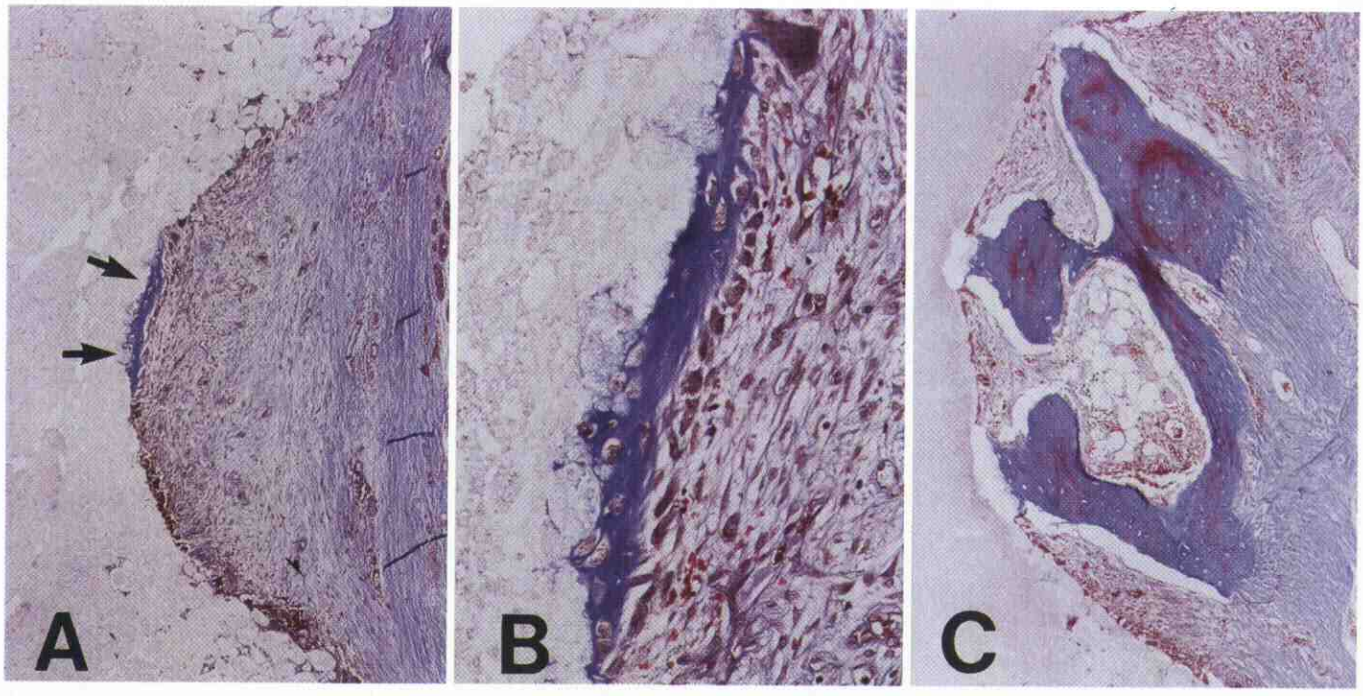

Fig. 3. Effect of geometry of the substratum on tissue morphogenesis. Monolithic discs of hydroxyapatite with concavities prepared on both outer surfaces were implanted in the rectus abdominis of the baboon and harvested on days 30 and 90 after surgery. **A**: Photomicrograph showing initiation of bone formation within a concavity of the hydroxyapatite substratum on day 30 (arrows). Note prominent angiogenesis and vascular invasion within the mesenchymal tissue of the concavity; **B**: higher magnification showing newly formed bone matrix surfaced by contiguous osteoblasts; **C**: detail of bone tissue that had formed in a concavity of the hydroxyapatite substratum 90 days after implantation. Note remodelling of the newly formed bone and generation of bone marrow (A: ×28, B: ×90, C: ×34).

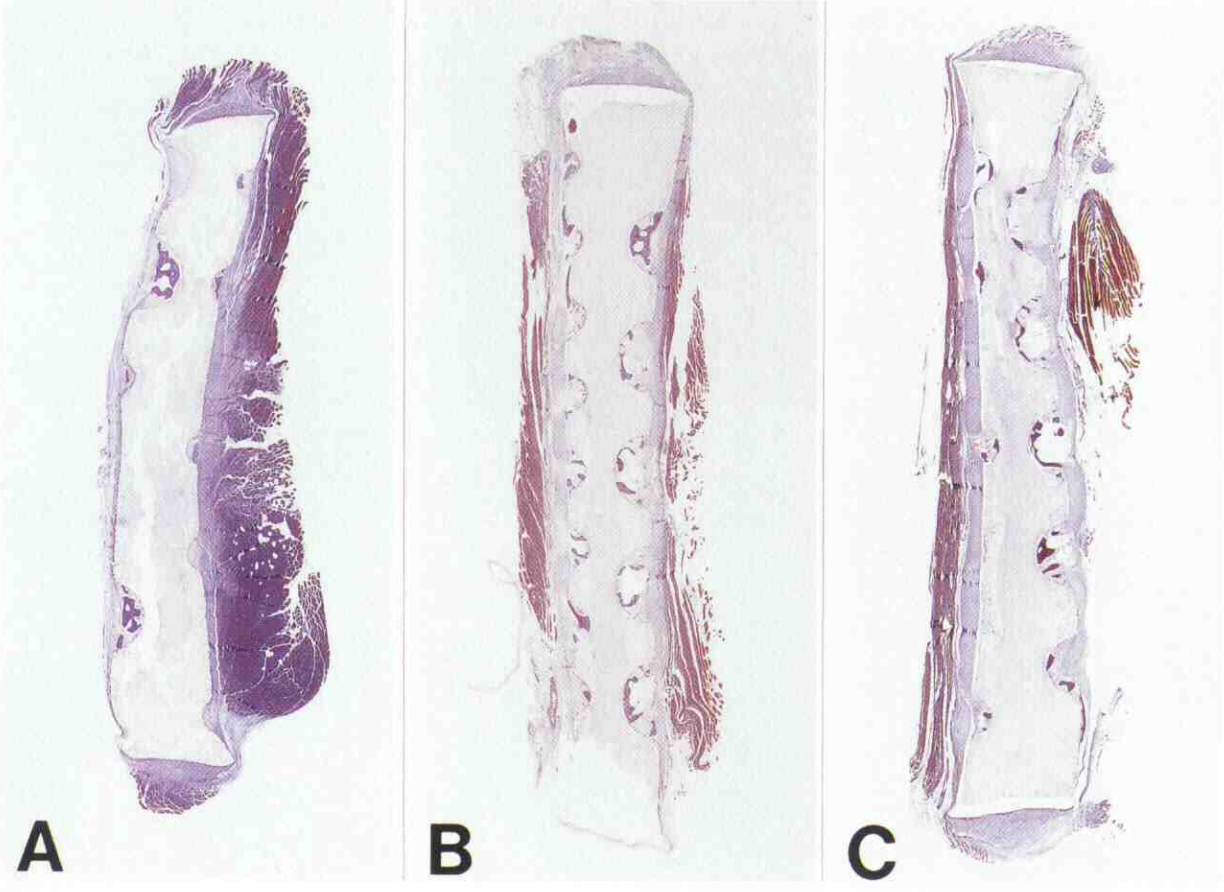

Fig. 4. Tissue morphogenesis in concavities of the substratum 90 days after heterotopic implantation. **A, B** and **C**: Low power view of histological sections of monolithic discs of sintered hydroxyapatite: bone has formed within all the available concavities prepared on both outer surfaces. Remodelling has occurred, resulting in the generation of large marrow lacunae (Fig. 3C for detail) (×5.8).

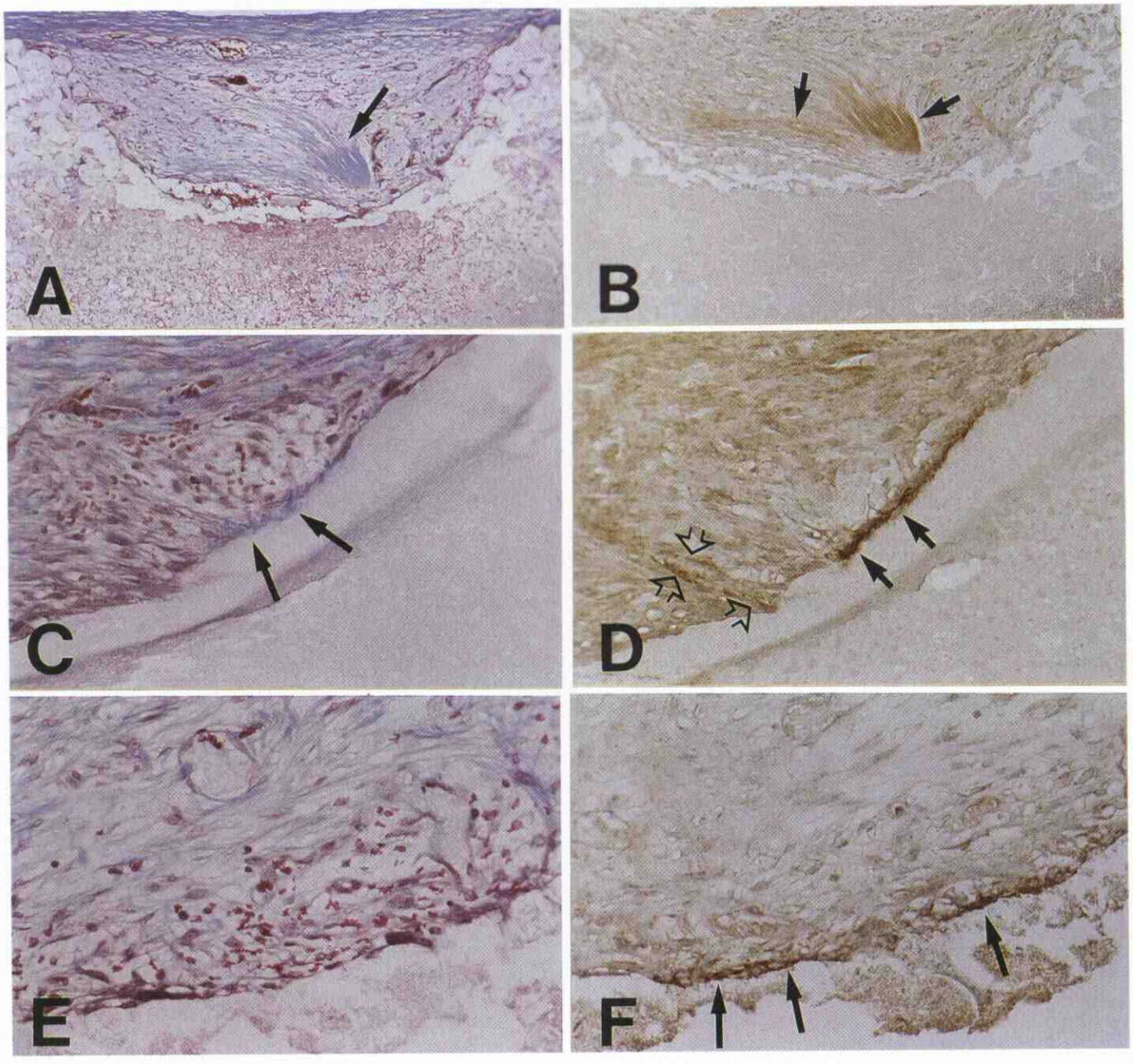

Fig. 5. Immunolocalization of BMP family members in mesenchymal tissue generated by concavities of the substratum on day 30 after implantation. **A**: Photomicrograph of a concavity with pronounced vascular invasion; generation of condensed collagenic material in close proximity to the interface (arrows); **B**: adjacent section showing immunolocalization of OP-1 (monoclonal antibodies) in the collagenic material (arrows). Additional serial sections stained with antibodies against BMP-2, -3 and -4 showed lack of immunoreactivity (not shown); **C**: detail of a concavity profile showing early morphogenetic events at the hydroxyapatite interface; note the generation and insertion of collagenic material directly onto the hydroxyapatite (arrows); **D**: adjacent section showing immunolocalization of OP-1 in the newly generated collagenic fibers at the interface (closed arrows), and in aligned cellular material in close proximity to the substratum (open arrows); **E**: tissue morphogenesis in an another concavity: angiogenesis, vascular invasion, and cellular differentiation at the hydroxyapatite interface; **F**: adjacent section showing immunolocalization of BMP-3 predominantly at the hydroxyapatite interface (arrows) (×56).

of the substratum. Histological analysis of serial sections suggested that bone never originated in close proximity to convex surfaces of hydroxyapatites. Bone first formed in direct apposition to concavities of sintered hydroxyapatite, and was lined by osteoblasts on its advancing surface (Fig. 6B, C). Histomorphometric analysis of generated tissues in porous sintered hydroxyapatites is summarized in Tables 1 and 2.

Calvarial repair by porous sintered hydroxyapatites

Representative histological sections of calvarial defects implanted with Plasma Biotal No. 3 and Tribo-Corr sintered hydroxyapatites harvested on day 90 are shown in Fig. 8. In three Plasma Biotal specimens, there was total penetration of bone within the porous spaces (Fig. 8A, B). However, in other Plasma Biotal specimens, there was substantial bone formation at the interfacial regions only, while the centre of the specimens showed limited bone growth, and the porous spaces were penetrated by dense fibrovascular tissue (Fig. 8C). Tribo Corr specimens generated new bone that reflected the geometry of porous spaces created during sintering (Fig. 8D). Histological analysis indicated a direct bonding of bone to both hydroxyapatites. Bone also formed on the external surfaces of the sintered hydroxyapatites, facing the pericranium and associated temporalis muscle (Fig. 8B). Contiguous osteoblasts lined the

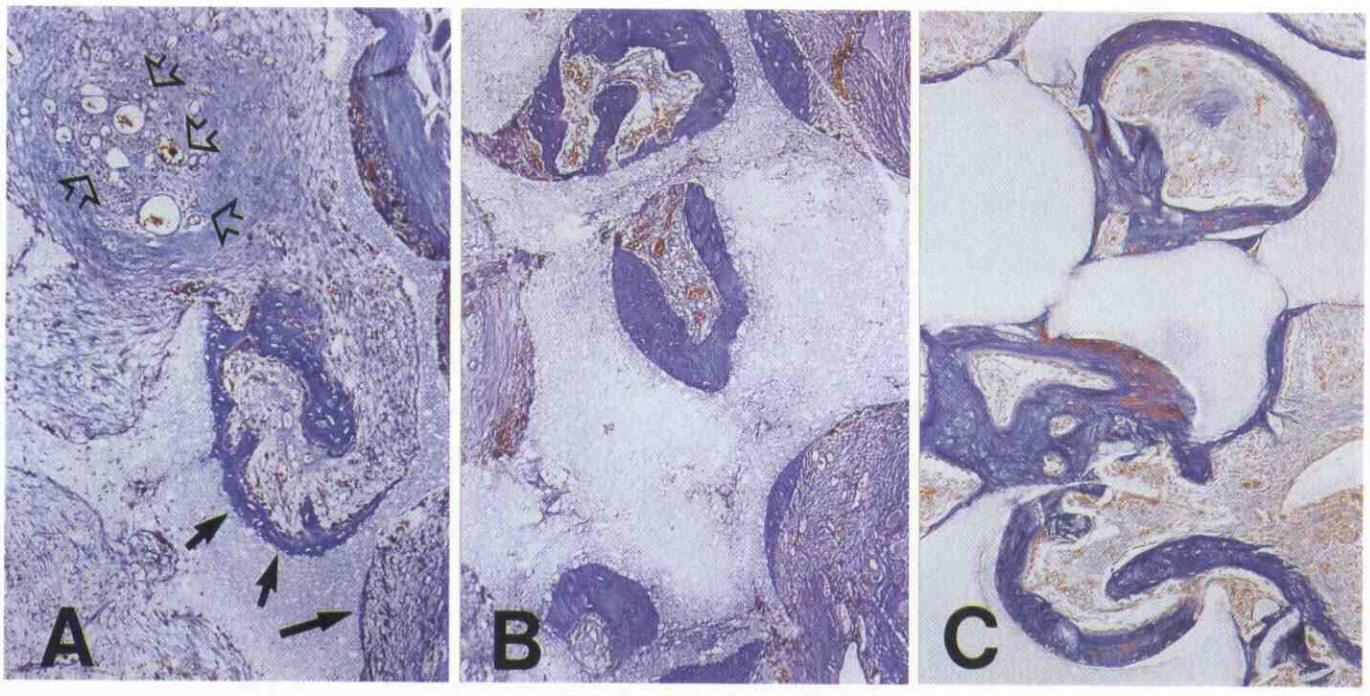

Fig. 6. Photomicrographs of porous sintered hydroxyapatites harvested from the rectus abdominis on day 30 (**A**) and 90 (**B** and **C**). **A**: Initiation of bone formation within two concavities of the porous hydroxyapatite (closed arrows); note prominent angiogenesis and vascular invasion within the mesenchymal tissue occupying the porous spaces of the hydroxyapatite implant (open arrows); **B** and **C**: extensive bone differentiation with remodelling in specimens of sintered porous hydroxyapatite harvested on day 90 (×28).

newly formed bone, which showed remodelling as indicated by the presence of lamellar, osteonic-like features.

Volume fraction compositions of calvarial specimens are presented in Table 3. There was no significant difference in bone volume generated by the Tribo-Corr and Plasma Biotal hydroxyapatites. In two Biotal specimens, bone volume was as high as 54 % and 62 %, respectively. A significantly greater amount of hydroxyapatite substratum was found in Tribo-Corr than in Plasma Biotal specimens ($P < 0.05$, Table 3). Comparison of the present results with those published previously using a coral-derived porous hydroxyapatite on day 90,[19] showed no significant differences in bone volume between the three series of hydroxyapatite specimens (31.2 ± 2.6 % in coral-derived hydroxyapatite).[19] Table 4 illustrates the distribution of bone and hydroxyapatite substratum within the five sources analysed by histomorphometry.

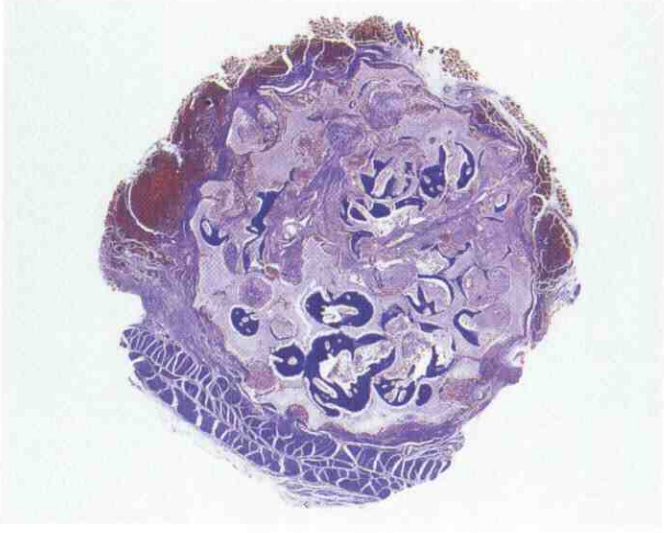

Fig. 7. Low power photomicrograph of porous sintered hydroxyapatites harvested from the rectus abdominis on day 90. Note bone formation (dark blue) within the porous spaces of the hydroxyapatite, and essentially confined to concavities of the substratum (×8).

Discussion

The findings reported in this article demonstrate the critical role of implant geometry in induction of bone by porous sintered hydroxyapatites implanted in heterotopic sites in the baboon. The molecular and cellular signals that trigger heterotopic osteoinduction in this animal are, however, poorly understood. Do BMPs/OPs in fact adsorb onto the hydroxyapatite substratum? Chromatographic adsorption of naturally derived mammalian BMPs onto gels of hydroxyapatite is a fundamental step in their purification.[20,26,32] Heterotopic bone differentiation in porous hydroxyapatites may be the result of adsorption of endogenously-produced BMPs and induction of bone as a secondary response. We found that radiolabelled hBMP-4 specifically bound to porous hydroxyapatite, and its binding *in vitro* was not affected by the geometry of the substratum.[15] A mechanism of adsorption of circulating or locally produced BMPs onto the hydroxyapatite substratum is further supported by the limited amount of bone induction on day 30, suggesting a lag period to attain a required critical concentration of BMPs for the initiation of bone formation. It is noteworthy that when using coral-derived porous hydroxyapatites, bone formation was never observed on day 30.[12] While substantial bone formation occurs by day 90, this lag period can be considerably shortened by pretreatment of coral-derived hydroxyapatites with BMPs, as demonstrated in orthotopic and heterotopic sites of the baboon.[19,33] In the present material, the immunolocalization of OP-1 and BMP-3 seems to reflect local expression and synthesis during the initial phases of tissue morphogenesis rather than proteins bound to the substratum from systemic circulation. Immunohistochemistry on sections representing earlier observation periods will be required to differentiate further between BMPs expressed at the interface or

bound to the substratum from systemic circulation.

Another question is why substratum geometry so profoundly influences tissue-specific gene expression. Our results demonstrate that concavities in the range of 400–1600 μm in diameter prepared in sintered hydroxyapatites regulate cell-specific differentiation culminating in the morphogenesis of bone. The importance of substratum geometry on cell shape, cell locomotion and cell differentiation has been demonstrated previously.[34] Tissue induction and morphogenesis can be greatly altered by the geometry of the substratum.[15,35–38] Earlier reports demonstrated the striking development of cartilage and bone in the lumen of glass tubes of a particular diameter when implanted in the dorsal subcutaneous space of the rat.[39] In more recent experiments, it was shown that the surface geometry of micro-machined substrata enhanced mineralized tissue formation *in vitro*, and influenced bone-like tissue formation *in vivo*.[40,41]

There may be several mechanisms by which the geometry of the substratum influences the expression of the osteogenic phenotype. The geometry may affect cellular morphology, and cellular shape will influence function.[42,43] While this concept has been amply demonstrated for cells cultured *in vitro* on various extracellular matrix components or micromachined substrata,[43–47] it is difficult to conceive a mechanism of control of cellular differentiation by macro-concavities of the substratum as in the present study. The establishment of a bone inductive microenvironment has been proposed following *in vitro* studies as well as results on heterotopic mineralization in rats.[41] The geometry of the substratum (concavities) may promote bone formation by providing porous spaces that are architecturally more conducive to processes culminating in bone differentiation. Angiogenesis and vascular invasion in the tissue generated within concavities were prominent histological features, which may also explain the lack of a chondrogenic phase during the morphogenesis of bone. In previous studies, using coral-derived hydroxyapatite, we suggested that the specific geometric and surface characteristics of the substratum induced rapid vessel ingrowth and capillary sprouting within the early mesenchyme that penetrated the porous spaces.[12] Histological, immunohistochemical and biochemical data suggested that *osteogenetic vessels*, as defined by Trueta in 1963,[48] might have provided a temporally regulated flow of cell populations capable of expression of the osteogenic phenotype.[12] The discovery of the affinity of BMP-3 and OP-1 (BMP-7) for type IV collagen[28,49] may link angiogenesis to osteogenesis, since type IV collagen is a major constituent of vascular basement membranes. Type IV collagen and other basement membrane components[49–51] may function as a delivery system by sequestering both angiogenic and bone morphogenetic proteins. Indeed, in recent studies on bone induction in primates using OP-1 (BMP-7) and transforming growth factor-β (TGF-β),[52,53] ossicles generated by combining OP-1 with TGF-β1 expressed a multiple increase in type IV collagen mRNA synthesis,[53] indicating that the two morphogens interacted synergistically to induce angiogenesis and vascular invasion,[52,53]

Table 1. Volume fraction composition (%) of specimens of sintered porous hydroxyapatite harvested on day 30 and 90 from the rectus abdominis of the baboon.

Treatment		Bone	Soft tissue	Substratum
Day 30				
Plasma Biotal	(10)	0.6 ± 0.3	71.2 ± 1.4	28.3 ± 1.3
Plasma Biotal P120	(4)	0.0	67.2 ± 3.1	32.8 ± 3.1
Tribo-Corr	(12)	0.2 ± 0.2	67.4 ± 0.7	32.4 ± 0.8
Day 90				
Plasma Biotal	(20)	2.7 ± 1.1	67.4 ± 1.5	29.3 ± 1.5
Plasma Biotal P120	(8)	13.2 ± 3.8	60.1 ± 3.5	26.7 ± 0.7
Tribo-Corr	(20)	3.0 ± 1.1	66.8 ± 1.6	30.2 ± 1.2
Plasmatex	(20)	4.4 ± 1.4	63.8 ± 1.8	31.8 ± 1.2
GR 500 P	(20)	7.2 ± 2.5	62.3 ± 2.5	30.5 ± 1.7

Volume fractions of tissue components were calculated using a Zeiss Integration Platte II with 100 lattice points superimposed over 2 serial sections per specimen as described in Materials and methods. Substratum indicates the implanted framework of the sintered hydroxyapatite. In brackets the number of specimens per treatment modality. Values (in %) are means ± s.e.m.

Table 2. Bone and hydroxyapatite volumes in the 41 % of specimens of porous sintered hydroxyapatite that showed osteoinductive activity on day 90 after implantation in the rectus abdominis of the baboon.

Treatment		Bone	Range	Substratum
Plasma Biotal	(7)	7.6 ± 1.9	2–14	29.8 ± 1.9
Plasma Biotal P120	(5)	15.9 ± 4.1	3–38	26.1 ± 0.8
Tribo-Corr	(7)	8.4 ± 1.9	3–16	29.8 ± 1.1
Plasmatex	(10)	8.7 ± 2.1	2–24	30.5 ± 1.7
GR 500 P	(12)	13.1 ± 3.6	2–33	27.4 ± 1.2

In brackets the number of specimens per treatment that showed bone induction on day 90. Values (in %) are means ± s.e.m.

Table 3. Volume fraction composition (%) of calvarial specimens harvested on day 90 from four adult baboons.

Source	Bone	Soft tissue	Substratum
Plasma Biotal	33.2 ± 2.7	48.5 ± 2.8	18.3 ± 1.9
Tribo-Corr	26.4 ± 2.6	47.9 ± 2.3	25.7 ± 1.7*

On day 90 after implantation, operated sites were perfused *in situ*, calvarial blocks harvested and serial decalcified sections, cut at 5 µm, were analysed by histomorphometry. Volume fractions of tissue components (in %) were calculated using the Zeiss Integration Platte II with 100 lattice points superimposed over 5 sources in each of 2 sagittal sections used for analysis as described in Materials and methods. Values are means ± s.e.m. of 8 calvarial specimens per group.
*$P < 0.05$ versus Plasma Biotal.

Table 4. Distribution of bone and hydroxyapatite substratum within histomorphometric sources in calvarial specimens of sintered hydroxyapatite harvested on day 90 from four adult baboons.

	Plasma Biotal		Tribo-Corr	
Source	Bone	Substratum	Bone	Substratum
AIF	46.4 ± 3.8	18.6 ± 2.1	34.7 ± 3.7	25.3 ± 2.1
AIN	30.2 ± 9.3	15.1 ± 2.5	26.3 ± 4.0	25.5 ± 2.3
CEN	26.3 ± 9.3	19.2 ± 1.5	21.4 ± 3.5	25.1 ± 1.8
PIN	22.3 ± 8.3	18.4 ± 2.1	22.9 ± 3.0	27.6 ± 1.5
PIF	40.4 ± 6.7	20.3 ± 2.8	26.9 ± 3.7	24.9 ± 1.8

Sources, as described in Methods, were: AIF: anterior interfacial; AIN: anterior internal; CEN: central; PIN: posterior internal; PIF: posterior interfacial. Values are means ± s.e.m. of 8 specimens per treatment modality.

as detected by a sharp increase in mRNA expression of type IV collagen.[53] A specific substratum geometry may thus restrict molecular initiators and responding cells within selected and confined spaces of the sintered hydroxyapatite, resulting in angiogenesis and, later, osteogenesis.

The finding of complete bone penetration in some calvarial specimens is noteworthy, and indicates that it is possible to construct sintered hydroxyapatites with interconnecting porous spaces throughout the discs. Interestingly, bone also formed on the external surfaces of the hydroxyapatite, facing the temporalis muscle, a histological feature not seen when using coral-derived hydroxyapatite implanted in an identical animal model.[18] An important point of discussion is the variability in the extent of bone formation in seemingly identical porous hydroxyapatites implanted both heterotopically and orthotopically. In heterotopic specimens, bone formation was substantial in some specimens, yet absent from others. The orthotopic specimens varied similarly. There was significant variability between animals with regard to bone induction in heterotopic specimens. This could be explained by different levels of circulating or locally produced BMPs in individual primates. Recent experiments have demonstrated the critical role of animal models in the morphogenesis of bone in porous hydroxyapatites.[13,54-56] The immunolocalization of OP-1(BMP-7) in basement membranes of epithelia and endothelium in the absence of detectable mRNA expression,[28] strongly indicates deposition within basement membranes at distance from sites of BMPs/OPs synthesis,[29,30] supporting the contention that specific BMPs/OPs bind to the porous hydroxyapatite from systemic circulation.

Further studies are required to elucidate the mechanisms of bone differentiation so as to construct sintered hydroxyapatites resulting in predictable osteoinduction throughout the available porous spaces. The discovery that specific geometric and surface characteristics of sintered hydroxyapatites can induce bone formation in heterotopic sites of primates paves the way for formulation and therapeutic application of 'smart' porous substrata designed to obtain predictable tissue types *via* intrinsic osteoinduction. The incorporation of specific biological activities into biomaterials achieved by manipulating the geometry of the substratum, defined as *geometric induction of bone formation*, may help to engineer therapeutic osteogenesis in clinical contexts.

This work is supported by the South African Medical Research Council, the University of the Witwatersrand and the CSIR. We thank B. van den Heever and M. Thomas for critical help during experiments.

Received 25 February. Accepted 10 April 1999.

1. Reddi A.H. (1994). Symbiosis of biotechnology and biomaterials: applications in tissue engineering of bone

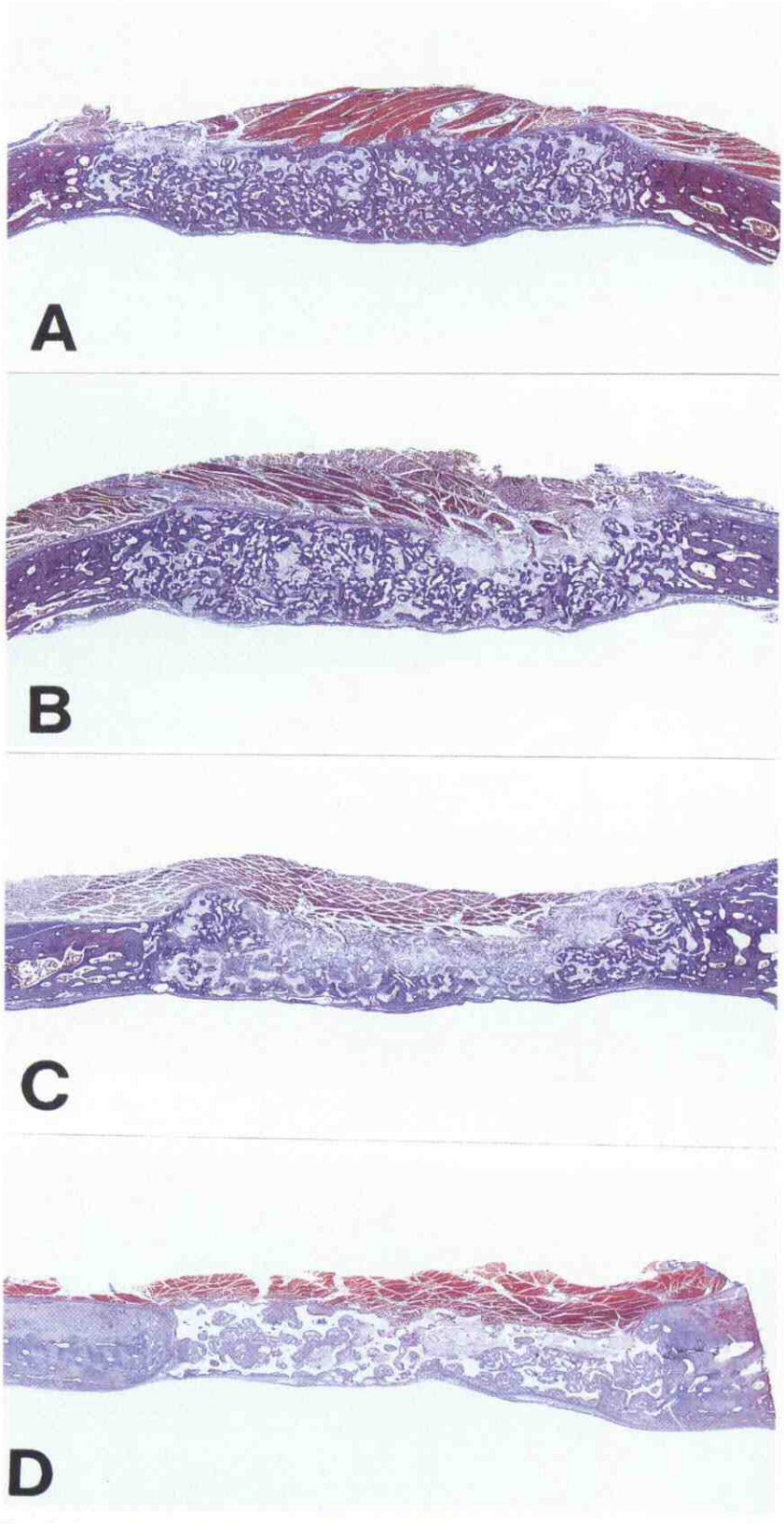

Fig. 8. Low power photomicrographs of orthotopic specimens of porous sintered hydroxyapatites prepared from Plasma Biotal No. 3 (**A, B** and **C**) and Tribo-Corr (**D**) powders as starting material. **A**: 90 days after implantation of the disc in a calvarial defect there is extensive and complete penetration of bone within the porous spaces; **B**: in another specimen of Plasma Biotal hydroxyapatite there is bone formation across the defect, but lack of bone penetration in a limited area subjacent to the temporalis muscle (arrows); **C**: bone formation at the periphery of another disc of Plasma Biotal, but lack of complete bone penetration across the porous spaces of the sintered hydroxyapatite; **D**: solid blocks of bone had formed within the available porous spaces 90 days after implantation of a Tribo Corr hydroxyapatite disc (×3.1).

and cartilage. *J. Cell. Biochem.* **56**, 192–195.
2. Ripamonti U. and Duneas N. (1996). Tissue engineering of bone by osteoinductive biomaterials. *Mat. Res. Soc. Bull.* **21**, 36–39.
3. Ripamonti U. and Reddi A.H. (1997). Tissue engineering and morphogenesis of periodontal tissues by bone morphogenetic proteins. *Crit. Rev. Oral Biol. Med.* **8**, 154–163.
4. Wozney J.M. (1992). The bone morphogenetic protein family and osteogenesis. *Molec. Reprod. Dev.* **32**, 160–167.
5. Reddi A.H. (1994). Bone and cartilage differentiation. *Curr. Opin. Genet. Dev.* **4**, 737–744.
6. Ripamonti U. and Vukicevic S. (1995). Bone morphogenetic proteins: from developmental biology to molecular therapeutics. *S. Afr. J. Sci.* **91**, 277–280.
7. Ripamonti U. and Duneas N. (1998). Tissue morphogenesis and regeneration by bone morphogenetic proteins. *Plast. Reconstr. Surg.* **101**, 227–239.
8. Jarcho M. (1981). Calcium phosphate ceramics as hard tissue prosthetics. *Clin. Orthop.* **157**, 259–278.
9. Hench L.L. and Wilson J. (1984). Surface-active biomaterials. *Science* **226**, 630–636.
10. Ripamonti U. (1990). Inductive bone matrix and porous hydroxyapatite composites in rodents and nonhuman primates. In *Handbook of Bioactive Ceramics, vol. II: Calcium Phosphate and Hydroxylapatite Ceramics*, eds T. Yamamuro, J. Wilson-Hench, L.L. Hench, pp. 245–253. CRC Press, Boca Raton.
11. Ripamonti U. (1991). The morphogenesis of bone in replicas of porous hydroxyapatite obtained from conversion of calcium carbonate exoskeletons of coral. *J. Bone Joint Surg.* **73-A**, 692–703.
12. Ripamonti U., Van den Heever B. and Van Wyk J. (1993). Expression of the osteogenic phenotype in porous hydroxyapatite implanted extraskeletally in baboons. *Matrix* **13**, 491–502.
13. Ripamonti U. (1996). Osteoinduction in porous hydroxyapatite implanted in heterotopic sites of different animal models. *Biomaterials* **17**, 31–35.
14. Van Eeden S. and Ripamonti U. (1994). Bone differentiation in porous hydroxyapatite is regulated by the geometry of the substratum: implications for reconstructive craniofacial surgery. *Plast. Reconstr. Surg.* **93**, 959–966.
15. Ripamonti U., Ma S. and Reddi A.H. (1992). The critical role of geometry of porous hydroxyapatite delivery system in induction of bone by osteogenin, a bone morphogenetic protein. *Matrix* **12**, 202–212.
16. Slosarczyk A. (1989). Highly porous hydroxyapatite material. *Powder Metall. Int.* **21**, 24–25.
17. Ripamonti U. (1991). Bone induction in nonhuman primates. An experimental study on the baboon (*Papio ursinus*). *Clin. Orthop.* **269**, 284–294.
18. Ripamonti U. (1992). Calvarial reconstruction in baboons with porous hydroxyapatite. *J. Craniofac. Surg.* **3**, 149–159.
19. Ripamonti U., Ma S., Van den Heever B. and Reddi A.H. (1992). Osteogenin, a bone morphogenetic protein, adsorbed on porous hydroxyapatite substrata, induces rapid bone differentiation in calvarial defects of adult primates. *Plast. Reconstr. Surg.* **90**, 382–393.
20. Ripamonti U., Ma S., Cunningham N.S., Yeates L. and Reddi A.H. (1992). Initiation of bone regeneration in adult baboons by osteogenin, a bone morphogenetic protein. *Matrix* **12**, 369–380.
21. Ripamonti U., Ma S., Cunningham N., Yeates L. and Reddi A.H. (1993). Reconstruction of the bone–bone marrow organ by osteogenin, a bone morphogenetic protein, and demineralized bone matrix in calvarial defects of adult primates. *Plast. Reconstr. Surg.* **91**, 27–36.
22. Ripamonti U., Van den Heever B., Sampath T.K., Tucker M.M., Rueger D.C. and Reddi A.H. (1996). Complete regeneration of bone in the baboon by recombinant human osteogenic protein-1 (hOP-1, bone morphogenetic protein-7). *Growth Factors* **13**, 273–289.
23. Parfitt A.M. (1983). Stereologic basis of bone histomorphometry; theory of quantitative microscopy and reconstruction of the third dimension. In *Bone Histomorphometry: Techniques and Interpretation*, ed. R.R. Recker, pp. 53–87. CRC Press, Boca Raton.
24. Parfitt A.M., Drezner M.K., Glorieux F.H., Kanis J.A., Malluche H., Meunier P.J., Ott S.M. and Recker R.R. (1987). Bone histomorphometry: standardization of nomenclature, symbols, and units. *J. Bone Miner. Res.* **2**, 595–610.
25. Hsu S.M., Raine L. and Fanger H. (1981). Use of avidin-biotin-peroxidase complex (ABC) in immunoperoxidase techniques: a comparison between ABC and unlabeled antibody (PAP) procedures. *J. Histochem. Cytochem.* **29**, 577–580.
26. Luyten F.P., Cunningham N.S. and Ma S. (1989). Purification and partial amino acid sequence of osteogenin, a protein initiating bone differentiation. *J. Biol. Chem.* **264**, 13377–13380.
27. Hammonds R.G., Schwall R., Dudley A., Berkemeir L., Lai C., Lee J., Cunningham N.S., Reddi A.H., Wood I, and Mason A.J. (1991). Bone inducing activity of mature BMP-2b produced from hybrid BMP-2a/2b precursor. *Mol. Endocrinol.* **5**, 149–155.
28. Vukicevic S., Latin V., Chen P., Batorsky R., Reddi A.H. and Sampath T.K. (1994). Localization of osteogenic protein-1 (bone morphogenetic protein-7) during human embryonic development: high affinity binding to basement membranes *Biochem. Biophys. Res. Commun.* **198**, 693–700.
29. Vukicevic S., Helder M.N. and Luyten F.P. (1994). Developing human lung and kidney are major sites for synthesis of bone morphogenetic protein-3 (osteogenin). *J. Histochem. Cytochem.* **42**, 869–875.
30. Helder M.N., Özkaynak E., Sampath T.K., Luyten F.P., Oppermann H. and Vukicevic S. (1995). Expression of osteogenic protein-1 (bone morphogenetic protein-7) in human and mouse development. *J. Histochem. Cytochem.* **43**, 1035–1044.
31. Statistical Analysis System (1989). *SAS/STATS User's Guide*, Version 6, 4th edn, vol. 1, pp. 209–244. SAS Institute, Cary.
32. Urist M.R., Huo Y.K and Brownell A.G. (1984). Purification of bovine bone morphogenetic protein by hydroxyapatite chromatography. *Proc. Natl. Acad. Sci. U.S.A.* **81**, 371–375.
33. Ripamonti U., Yeates L. and Van den Heever B. (1993). Initiation of heterotopic osteogenesis in primates after chromatographic adsorption of osteogenin, a bone morphogenetic protein, onto porous hydroxyapatite. *Biochem. Biophys. Res. Commun.* **193**, 509–517.
34. Reddi A.H. (1974). Bone matrix in the solid state: geometric influence on differentiation of fibroblasts. *Adv. Biol. Med. Phys.* **15**, 1–18.
35. Reddi A.H. and Huggins C.B. (1973). Influence of geometry of transplanted tooth and bone on transformation of fibroblasts. *Proc. Soc. Exp. Biol. Med.* **143**, 634–637.
36. Sampath T.K. and Reddi A.H. (1984). Importance of geometry of the extracellular matrix in endochondral bone differentiation. *J. Cell Biol.* **98**, 2192–2197.
37. Kuboki Y., Saito T., Murata M., Takita H., Mizuno M., Inoue M., Nagai N. and Poole A.R. (1995). Two distinctive BMP-carriers induce zonal chondrogenesis and membranous ossification, respectively: geometrical factors of matrices for cell-differentiation. *Connect. Tissue Res.* **32**, 219–226.
38. Kuboki Y., Takita H., Kobayashi D., Tsuruga E., Inoue M., Murata M., Nagai N., Dohi Y. and Ohgushi H. (1998). BMP-induced osteogenesis on the surface of hydroxyapatite with geometrically feasible and nonfeasible structures: topology of osteogenesis. *J. Biomed. Mat. Res.* **39**, 190–199.
39. Selye H. (1960). Induction of bone cartilage and hemopoietic tissue by subcutaneously implanted tissue diaphragms. *Roux' Archiv. Entwicklungsmechanik.* **151**, 572–585.
40. Brunette D.M., Ratkay J. and Chehroudi B. (1991). The behaviour of osteoblasts on micromachined surfaces. In *The Bone-Biomaterial Interface*, ed. J.E. Davies, pp. 170–180. University of Toronto Press, Toronto.
41. Chehroudi B., Ratkay J. and Brunette D.M. (1992). The role of implant surface geometry in mineralization *in vivo* and *in vitro*: a transmission and scanning electron microscopic study. *Cells Mater.* **2**, 89–104.
42. Singhvi R., Stephanopolous G. and Wang D.I.C. (1993). Review: Effects of substratum morphology on cell physiology. *Biotech. Bioeng.* **43**, 764–771.
43. Folkman J. and Greenspan H.P. (1975). Influence of geometry on control of cell growth. *Biochem. Biophys. Acta* **417**, 211–236.
44. Gospodarowicz D., Greenburg G. and Birdwell C.R. (1978). Determination of cellular shape by the extracellular matrix and its correlation with the control of cellular growth. *Cancer Res.* **38**, 4155–4171.
45. Bissell M.J. and Barcellos-Hoff M.H. (1987). The influence of extracellular matrix on gene expression: is structure the message? *J. Cell Sci. Suppl.* **8**, 327–343.
46. Inoue T., Cox J.E., Pilliar R.M. and Melcher A.H. (1987). Effect on the surface geometry of smooth and porous-coated titanium alloy on the orientation of fibroblasts *in vitro*. *J. Biomed. Mater. Res.* **21**, 107–126.
47. Brunette D.M. (1988). The effects of implant surface topography on the behaviour of cells. *Int. J. Oral Maxillofac. Impl.* **3**, 231–246.
48. Trueta J. (1963). The role of the vessels in osteogenesis. *J. Bone Joint Surg.* **45-B**, 402–418.
49. Paralkar V.M., Nandekar A.K.N., Pointer R.H., Kleinman H.K. and Reddi A.H. (1990). Interaction of osteogenin, a heparin binding bone morphogenetic protein, with type IV collagen. *J. Biol. Chem.* **265**, 17281–17284.
50. Paralkar V.M., Vukicevic S. and Reddi A.H. (1991). Transforming growth factor β type 1 binds to collagen IV of basement membrane matrix: implications for development. *Dev. Biol.* **143**, 303–308.
51. Vlodavsky I., Folkman J., Sullivan R., Fridman R., Ishai-Michaeli R., Sasse J. and Klagsbrun M. (1987). Endothelial cell-derived basic fibroblast growth factor: synthesis and deposition into subendothelial extracellular matrix. *Proc. Natl. Acad. Sci. U.S.A.* **84**, 2292–2296.
52. Ripamonti U., Duneas N., Van den Heever B., Bosch C. and Crooks J. (1997). Recombinant transforming growth factor-β1 induces endochondral bone in the baboon and synergizes with recombinant osteogenic protein-1 (bone morphogenetic protein-7) to initiate rapid bone formation. *J. Bone Min. Res.* **12**, 1584–1595.
53. Duneas N., Crooks J. and Ripamonti U. (1998). Transforming growth factor-β1: Induction of bone morphogenetic protein genes expression during endochondral bone formation in the baboon, and synergistic interaction with osteogenic protein-1 (BMP-7). *Growth Factors* **15**, 259–277.
54. Yang Z., Yuan H., Tong W., Zou P., Chen W. and Zhang X. (1996). Osteogenesis in extraskeletally implanted porous calcium phosphate ceramics: variability among different kinds of animals. *Biomaterials* **17**, 2131–2137.
55. Yamasaki H. and Sakai H. (1992). Osteogenic response to porous hydroxyapatite ceramics under the skin of dogs. *Biomaterials* **13**, 308–312.
56. Klein C., De Groot K., Weiqun C., Yubao L. and Xingdong Z. (1994). Osseous substance formation induced in porous calcium phosphate ceramics in soft tissues. *Biomaterials* **15**, 31–34.

29

Copyright of South African Journal of Science is the property of South African Assn. for the Advancement of Science and its content may not be copied or emailed to multiple sites or posted to a listserv without the copyright holder's express written permission. However, users may print, download, or email articles for individual use.